J. Fluid Mech. (2005), *vol.* 538, *pp.* 111–136. © 2005 Cambridge University Press
doi:10.1017/S002211200500515X Printed in the United Kingdom

Starting flow through nozzles with temporally variable exit diameter

By JOHN O. DABIRI AND MORTEZA GHARIB

Graduate Aeronautical Laboratories & Bioengineering, California Institute of Technology, Pasadena, CA 91125, USA

(Received 21 June 2004 and in revised form 10 March 2005)

Starting flow through a nozzle or orifice typically results in the transient formation of a leading vortex ring and trailing jet. Experiments are conducted to investigate the dynamics of this process in the case of a temporally variable nozzle exit diameter, with the aim of understanding these flows as they occur in Nature and emerging technologies. By kinematically decoupling the source flow from the nozzle motion, comparison across several classes of exit diameter temporal variation is facilitated. Kinematic models of the starting flows are used to accurately predict the fluid circulation produced by the vortex generators, and to emphasize the special role of the nozzle boundary layer in dictating the nature of the global flow patterns. A dimensionless temporal parameter is derived in order to track the vortex formation process for the various classes of nozzle motion. Dynamics of vortex ring disconnection from the source flow are studied in this new dimensionless framework. We show that temporally increasing the nozzle exit diameter as the starting flow develops results in higher-energy vortex ring structures with peak vorticity located further from the axis of symmetry relative to a static nozzle case. In addition, the normalized energy supplied by the vortex generator is increased in this process. We do not observe a delay in the onset of vortex ring disconnection from the trailing jet, as predicted by previous numerical simulations. In contrast, growth of the leading vortex ring is substantially augmented by temporally decreasing the nozzle exit diameter during fluid ejection, as noted in a previous experiment. Normalized vortex ring circulation is increased 35 % in these cases, and the normalized energy of the generated vortex rings is equivalent to that of Hill's spherical vortex. These observed effects are explained by considering the measured vorticity distribution and energy of the starting flows. Strategies are suggested to exploit the discovered dynamics for various pulsed-jet applications.

1. Introduction

Pulsatile flows are among the most common and successful mechanisms for convective fluid transport found in Nature. Although the selection of such techniques may often be related to morphological constraints (Vogel 1988, 1994), it remains noteworthy that today we can observe the action of these unsteady flows in systems ranging from the most primitive jellyfish locomotor to the complex trans-mitral and trans-aortic blood flows in the animal heart.

Throughout the diverse catalogue of biological systems using pulsatile flow, the generated starting flow typically emerges from a nozzle or orifice with temporally variable exit diameter. In systems with valve structures governing the flow, the

https://doi.org/10.1017/S002211200500515X Published online by Cambridge University Press

observed motion of the exit diameter is a necessary consequence of the transition from a closed valve to an open one, and *vice versa*. An important example is the animal heart, where it has been suggested that the interaction between the starting flows and the moving valves can be correlated to some commonly observed cardiac pathologies (e.g. Gorman *et al.* 1996; Yogonathan, Lemmon & Ellis 2000; Handke *et al.* 2003).

In addition to the aforementioned use of starting flows for mass transfer, many biological systems have coopted pulsatile flow for locomotion. Certain cnidarians (e.g. jellyfish), cephalopods (e.g. squid), and bivalves (e.g. scallops) are most prominent in this regard. Dabiri & Gharib (2003) measured exit diameter changes up to 30 % during steady swimming of *Chrysaora fuscescens* jellyfish. Transient exit diameter changes of over 400 % have been measured in the *Lolliguncula brevis* squid (Bartol, Patterson & Mann 2001), and the nozzle exit has been observed to close completely between fluid pulses in the *Loligo pealei* squid (Anderson & DeMont 2000). In many instances, the temporal variation of the exit diameter is actively controlled, suggesting possible real-time refinement of the fluid–structure interaction.

The fluid dynamical effect of a temporally variable nozzle exit diameter on a starting flow has remained essentially unexplored. Our motivation for this study is at least twofold. First, a better understanding of these systems can facilitate predictive models to explain correlations between local fluid–structure interactions at the nozzle or orifice exit and observed global features of the generated flow. Secondly, we may explain the physical impetus for the specific programmes of exit diameter temporal variation observed in Nature. The design principles that are elucidated here may be transferable to emerging engineering technologies, such as pulsed-jet propulsors and synthetic jets (see Glezer & Amitay 2002 for a review).

From a kinematic perspective, the primary constituents of the starting flow through a nozzle or orifice are a leading vortex ring and, in some cases, a trailing jet. A large literature dealing with the dynamics of the quasi-steady jet is now available; however, our understanding of the dynamics of the leading vortex ring is more limited. Gharib, Rambod & Shariff (1998) experimentally identified a transition from formation of a single vortex ring to generation of a leading vortex ring and trailing flow, as a function of the normalized length of the ejected slug of fluid. Their work and subsequent models by Mohseni & Gharib (1998), Linden & Turner (2001), and Mohseni (2001) have pointed to the effect of an energetic requirement for the leading vortex ring during this transition, as stipulated by the Kelvin–Benjamin variational principle (Kelvin 1875; Benjamin 1976). The principle suggests that the leading vortex ring is incapable of further growth via ingestion of fluid from the vortex generator if the energy of this source flow falls below the vortex ring energy. Dynamical separation of the leading vortex ring from the trailing flow owing to this energetic effect is referred to as *pinch-off* in the literature.

Krueger (2001) and Krueger & Gharib (2003) attained the first measurements of the dynamical effect of the vortex ring pinch-off process. They discovered that the time-averaged force generated by a starting flow becomes maximal at the onset of vortex ring pinch-off. This result suggests an optimal operating point just before vortex ring pinch-off, and also motivates the search for methods to delay vortex ring pinch-off altogether. Dabiri & Gharib (2004*a*) successfully demonstrated the possibility of delaying vortex ring pinch-off, by imposing an external axisymmetric counterflow during vortex ring formation. Although those experiments demonstrated the feasibility of delaying vortex ring pinch-off in general, it would be more useful to

https://doi.org/10.1017/S002211200500515X Published online by Cambridge University Press

achieve similar results by manipulating properties of the vortex ring generator itself, i.e. in the absence of external intervention.

Numerical studies by Rosenfeld, Rambod & Gharib (1998) Zhao, Frankel & Mongeau (2000) and Mohseni, Ran & Colonius (2001) have demonstrated that parameters such as shear-layer thickness, Reynolds number, and velocity profile can all affect the dynamics of the pinch-off process. As this parameter space has only been explored in numerical simulations, it is not immediately evident how each of these parameters should be manipulated in practice. Nevertheless, two practical methods have emerged from the simulations of Mohseni *et al.* (2001) as potential candidates to delay pinch-off of the leading vortex ring. In the first case, it is suggested that the velocity of the source flow from the vortex generator be increased to prolong feeding of dynamical invariants (i.e. energy, impulse and circulation) to the leading vortex ring. This concept is also proposed by Shusser & Gharib (2000) as a corollary to their theory that vortex ring pinch-off occurs when the velocity of the trailing jet (source flow) falls below the celerity of the leading vortex ring.

The second method suggested by Mohseni *et al.* (2001) is to increase the radial extent of the forcing (i.e. increase the nozzle or orifice exit diameter) as the starting flow emerges from the vortex generator. In this way, the shear layer of the source flow behind the leading vortex ring could be moved away from the axis of symmetry, where it would normally cancel with its mirror across the azimuthal plane of symmetry and lose strength.

These and other potential methods for pinch-off delay have not yet been validated experimentally. J. J. Allen (New Mexico State University 2003, personal communication) has conducted experiments on vortex ring formation with a variable diameter orifice aperture. Consistent with the prediction of Mohseni *et al.* (2001), preliminary results indicated the effectiveness of an accelerating source flow for generating vortex rings of low normalized energy, possibly indicative of delayed vortex ring pinch-off. In contrast, increasing the radial extent of the forcing via a temporally increasing orifice aperture did little to enhance the vortex ring formation process. Several questions remain unanswered regarding the experimental method of Allen, including the effects of fluid structures generated on the upstream-facing side of the orifice plate (e.g. in stagnation zones); aperture rotation about the axis of symmetry during orifice enlargement; and non-circular aperture shape. Hence, we will only refer to those experiments in regard to the general qualitative trends observed.

The objective of the present experiments is to study the dynamics of starting flows through nozzles with temporally variable exit diameter. The nearly axisymmetric nozzle used in these experiments serves as a generalization of the various nozzle and orifice geometries observed in biological systems. Nozzle dynamics are decoupled from the source flow by imposing a constant volume flux from a piston–cylinder apparatus at the inlet to the nozzle during all experiments. This strategy proves to simplify the analysis and facilitate quantitative comparison across all of the test cases. An important goal of these experiments is to implement the strategies for pinch-off delay suggested by Mohseni *et al.* (2001) and examined by Allen. The observed starting flow dynamics are explained in terms of the shear-layer kinematics and leading vortex ring vorticity distribution and energy. In addition, we examine relevant measures of pulsing performance to suggest benefits of temporally variable nozzle and orifice exit diameters in biological systems and emerging technologies.

The following section describes the apparatus and experimental methods in detail, with special attention given to possible artefacts that could be introduced to the

https://doi.org/10.1017/S002211200500515X Published online by Cambridge University Press

observed fluid dynamics by the nature of the nozzle design. The results are catalogued in § 3, beginning with the kinematics of the nozzle boundary layer and shear-layer efflux, and subsequently focusing on the dynamics of the leading vortex ring. Nuances of dimensional analysis for the time-dependent exit diameter are also presented in this section. Section 4 summarizes the analyses, provides comparison with previous numerical and experimental observations of these flows, and discusses the physical basis for effective use of temporally varying exit diameters in practice.

2. Apparatus and experimental methods

2.1. *Apparatus design*

Several challenges were faced in designing an apparatus to achieve temporal variation of a nozzle exit diameter, without introducing undue complexity or unwanted artefacts into the experiments. The design requirements included – but were not limited to – distinct and repeatable separation of the nozzle boundary layer at a known radial distance from the axis of symmetry and at a fixed axial location; a nozzle wall that is sufficiently rigid to prevent deformation due to fluid forces, yet flexible enough to vary the exit diameter over a large range; uniform radial actuation to maintain a nearly circular shape at the nozzle exit plane; suppression of secondary vorticity generation by the apparatus (e.g. as is present on the upstream-facing side of an orifice plate); and an actuation mechanism that does not measurably disturb the flow.

This set of requirements is appropriately satisfied by the apparatus represented in figure 1. The source flow is generated by a traditional piston–cylinder apparatus (cf. Dabiri & Gharib 2004*c*), with the inlet flow originating from the left-hand side of the hollow cylinder (inner diameter = 2.5 cm) in the schematic. A piston is oriented coaxially with the hollow cylinder and has its diameter D_p flush with the inner surface of the cylinder. The piston is driven by flow supplied from an external constant-head tank operating at a total pressure head Δp of 8.2 kPa. A computer-controlled solenoid valve meters the flow using an impulsive velocity profile with a rise time of approximately 300 ms to steady flow at 8.8 $\mathrm{cm^3\,s^{-1}}$. Flow rates are monitored by an ultrasonic flow probe at the inlet to the cylinder and are recorded to a computer hard disk via a LabVIEW program. A single value of the constant volume flux is used throughout all of the experiments described in this paper. In this way, the source flow merely serves as a control parameter and falls out of much of the subsequent analyses. Source flow from the piston–cylinder apparatus enters the nozzle inlet, which is mounted immediately downstream.

The nozzle is constructed from a 5.1 cm length of originally straight latex rubber tubing with 1.5 cm nominal inner diameter, 0.08 cm nominal thickness, and sharp edges. Optimal wall thickness was determined from repeated iterations of the design to facilitate maximum actuation of the exit diameter without becoming susceptible to deformation due to fluid forces. The nozzle inlet diameter is matched to the inner diameter of the upstream hollow cylinder, by fitting the elastic tube over the outer diameter of the cylinder lip (D_o = 3.1 cm). To facilitate a smooth transition from the cylinder to the nozzle, the cylinder lip is sharpened to form a 7° wedge from its outer diameter to inner diameter (cf. figure 1 of Dabiri & Gharib 2004*c*). The nozzle is held to the cylinder by elastic forces induced during the process of stretching the latex tube over the cylinder lip, and by a series of compression clamps placed around the cylinder outer diameter.

For simplicity in later analyses, a spatially linear contraction in nozzle diameter from the inlet to the exit plane is desired. This is accomplished by supporting the

https://doi.org/10.1017/S002211200500515X Published online by Cambridge University Press

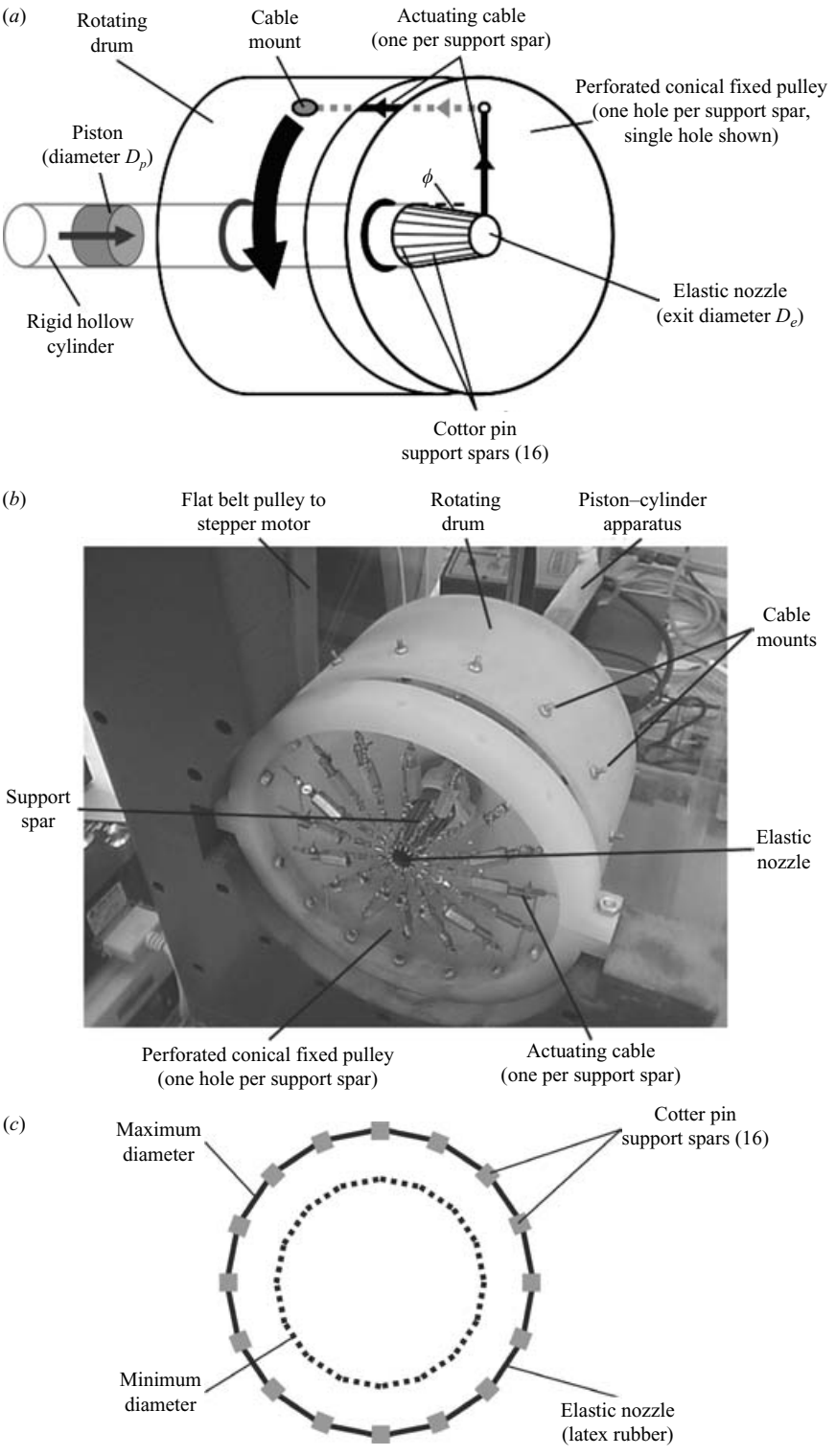


FIGURE 1. Apparatus for temporal variation of nozzle exit diameter. (*a*) Schematic. (*b*) Laboratory image. (*c*) Front view of nozzle exit plane.

https://doi.org/10.1017/S002211200500515X Published online by Cambridge University Press

elastic nozzle with 16 straight stainless steel cotter pin support spars equally spaced azimuthally around the nozzle. Each support spar has a hairpin shape, and is fitted over the downstream edge of the elastic nozzle with both prongs extending upstream along the length of the nozzle. The junction of the two prongs of each hairpin is positioned at the nozzle exit plane. The free ends of the two prongs of each hairpin are fixed to the inner and outer surfaces of the nozzle, respectively, using a waterproof adhesive. These free hairpin ends effectively act as a pin joint when the nozzle is actuated.

A water-resistant actuating cable is connected to the hairpin junction of each support spar at the nozzle exit plane; the cable extends radially to a perforated conical shell that acts as a fixed pulley. The apex of the cone is truncated, and the piston–cylinder apparatus is mounted rigidly through the apical opening. After passing through a hole in the wall of the conical fixed pulley, the cable is turned 90° toward an axial orientation upstream, where its terminal end is mounted to the inner surface of a hollow drum. The drum is mounted coaxially to the piston–cylinder apparatus on a roller bearing, so that it is free to rotate about the axis of symmetry.

When the drum rotates, the terminal end of the cable that is mounted to the drum moves azimuthally. Since the cable is inextensible, the other end of the cable connected to the support spar is pulled radially toward its respective hole in the conical pulley. By this mechanism, a single degree of freedom in the rotating drum is transduced to radial actuation at 16 uniformly spaced locations around the azimuth of the nozzle exit plane.

A flat-belt pulley system connects the drum to a computer-controlled stepper motor that governs the nozzle motion. The drum rotation necessary for actuation of the nozzle from minimum to maximum diameter is approximately 30°. Details of the specific programs of exit diameter variation used in these experiments will be presented in a subsequent section.

The entire piston–cylinder–nozzle apparatus is submerged in a 60 cm high × 40 cm wide × 100 cm long water tank with transparent walls. Mounting points are located along the cylinder and around the azimuth of the conical pulley.

2.2. *Effects of non-circular nozzle shape*

Although most of the design requirements are satisfied by the apparatus described above, an important concern must be directly addressed regarding the shape of the nozzle exit. Figure 1(*c*) shows the front view of the nozzle at the exit plane, in proportions that are approximately to scale. The cotter pin support spars, with dimensions of 0.13 cm azimuthally and 0.08 cm per prong radially, act as a finite-amplitude disturbance with wavenumber 16 on the starting flow. It is reasonable to question the behaviour of this disturbance in time, especially as it relates to the forming leading vortex ring.

The stability theory for an exact representation of this flow is unresolved and also beyond the scope of this paper. However, we can appeal to the classical inviscid theory and make use of qualitative experiments to develop a convincing argument for the negligible effect of the nozzle shape perturbations on the flow.

Azimuthal wave development on vortex rings has been appreciated for decades, beginning with the experimental work of Krutzsch (1939). The physics of the phenomenon were elucidated by Widnall, Bliss & Tsai (1974), and further refined by Widnall & Tsai (1977), Saffman (1978) and Shariff, Verzicco & Orlandi (1994). The work of Saffman (1978) is especially useful in the present context, as it examines the dependence of the most unstable wavenumber on the Reynolds number (based

https://doi.org/10.1017/S002211200500515X Published online by Cambridge University Press

on ring celerity and nozzle exit diameter) and diameter-normalized length of the ejected slug of fluid T^*. Combining equations (4.4) and (4.6) of his paper leads to a relationship between the most unstable wavenumber, the critical Reynolds number and the parameter T^*. The equations predict that the growth of azimuthal disturbances of large wavenumber is suppressed at low Reynolds numbers. For the normalized fluid slug length in the vortex rings studied here ($T^* \leqslant 8$), the Reynolds number corresponding to an unstable wavenumber 16 (i.e. $Re \approx 6 \times 10^4$) is approximately two orders of magnitude higher than the conditions of the present experiments.

We note that this is a simplified calculation. To further support the above conclusion, we conducted dye-visualization experiments of the starting jet formed by the apparatus at the minimum and maximum nozzle exit diameter. In both cases, the vortex ring remained laminar and did not retain visible signs of the shape perturbation at the nozzle exit (at wavenumber 16 or otherwise), throughout observation of the rings until the dye began to dissipate far downstream. Especially in light of the fact that our observations will focus on the near-field flow, we proceed under the assumption that the measured dynamics do not represent artefacts from non-idealities in the experimental apparatus. The nozzle exit diameter in each case is defined based on an equivalent circle with cross-sectional area equal to the measured nozzle exit area.

2.3. *Quantitative flow visualization*

Kinematics of the flow field are measured using digital particle-image velocimetry (DPIV, cf. Adrian 1991; Willert & Gharib 1991). The hardware and parameters of the technique are essentially the same as described in Dabiri & Gharib (2004*c*). A laser sheet from a Nd:YAG laser source illuminates a plane of symmetry relative to the vortex generator, providing an azimuthal view of the axisymmetric starting flow from an orthogonally-oriented digital CCD camera at 30 Hz. In the present experiments, the flow field measures 7.8 cm (3.1 D_p) radially from the axis of symmetry; and from 0.77 cm (0.3 D_p) to 15.8 cm (6.2 D_p) downstream. The field is imaged at a resolution of approximately 65 pixels per cm, sufficient to resolve the vorticity distribution in the vortex ring core.

Timing of source flow initiation, nozzle actuation, laser firing and image capture is coordinated by an in-house code and LabVIEW data acquisition hardware. Velocity and vorticity measurements possess an uncertainty of 1 % and 3 %, respectively.

2.4. *Experimental parameter space*

The extreme positions of the nozzle exit diameter are plotted to approximate scale in figure 1(*c*). The maximum nozzle exit area is nearly 200 % of the minimum exit area. These positions are the end points of the temporal exit diameter variation in each of the experiments conducted. Figure 2 plots the specific programmes of nozzle exit diameter variation studied in these experiments. The diameter profiles were measured from frontal view video recordings of the nozzle undergoing each actuation program. The measured diameter at each instant is an effective value computed as $D_e = 2(A_e/\pi)^{1/2}$, where A_e is the nozzle exit area. This method accounts for the reduced nozzle exit area due to the presence of cotter pin support spars at the exit plane (i.e. their thickness and orientation; see figure 1*c*), and is the source of the lower minimum exit diameter (i.e. $D_e = 1.21$ cm) relative to the nominal pre-installation tube diameter (i.e. $D_e = 1.5$ cm). Static nozzle cases at minimum ($D_e = 1.21\,\text{cm} = 0.48\ D_p$; hereinafter SMIN) and maximum ($D_e = 1.69\,\text{cm} = 0.67\ D_p$; hereinafter SMAX) diameter are included as control sets. The dynamic nozzle cases consist of a slower-opening (SO) case, a faster-opening (FO) case, a slower-closing (SC) case, and a faster-closing (FC) case.

https://doi.org/10.1017/S002211200500515X Published online by Cambridge University Press

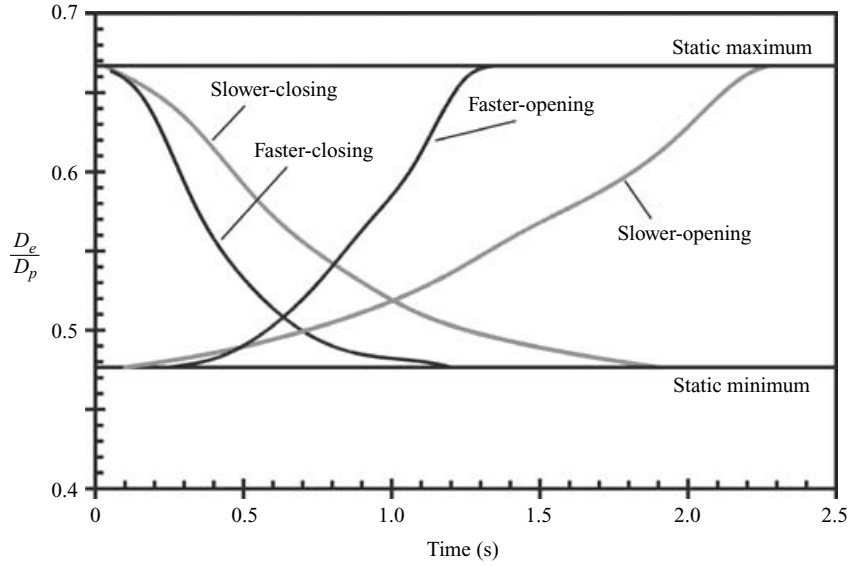


FIGURE 2. Programmes of nozzle exit diameter temporal variation.

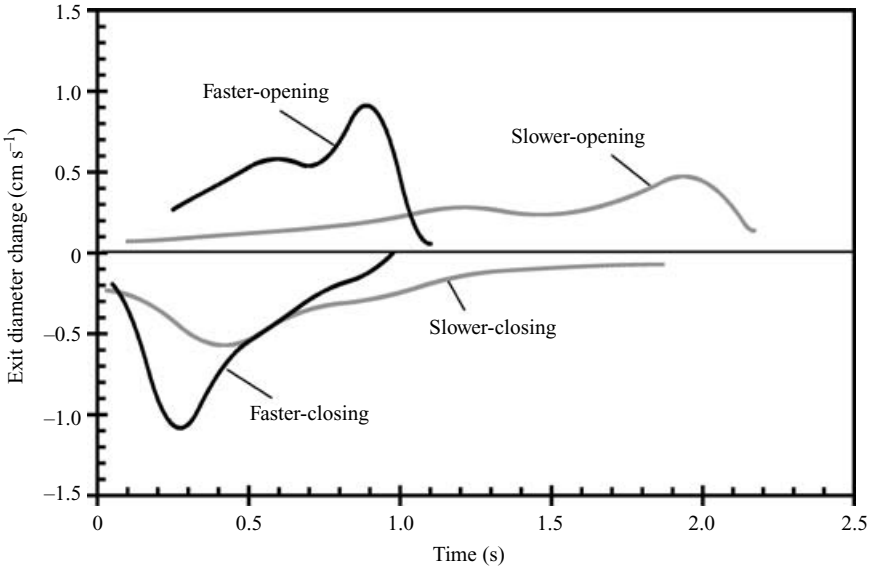


FIGURE 3. Rate of diameter change for each programme of nozzle exit diameter temporal variation.

The time derivative of the nozzle exit diameter change is shown in figure 3. These plots indicate that the peak temporal variation in the faster cases is double that of the slower cases. The slight modulation in nozzle exit diameter rate of change for the SO and FO cases (at time $t = 1.2$ s and 0.6 s, respectively) occurred owing to artefacts related to elastic deformation of the nozzle by the support spars, but did not measurably affect the observed vortex dynamics. Dynamic nozzle programs are repeatable to within 3 %.

https://doi.org/10.1017/S002211200500515X Published online by Cambridge University Press

Nozzle contraction angle ϕ varies between 12° degrees when the exit diameter is in its maximum position, and 18° when in its minimum position.

The Reynolds numbers at which these experiments were conducted range between 660 and 920 based on the nozzle exit velocity ($3.9\,\mathrm{cm\,s^{-1}} < U_e < 7.7\,\mathrm{cm\,s^{-1}}$) and diameter, and between 1500 and 3500 based on the circulation of the leading vortex ring. These Reynolds numbers are consistent with several of the biological systems discussed in § 1, such as jellyfish (Daniel 1983; Dabiri & Gharib 2003) and juvenile squid (Bartol *et al.* 2001), but are below the range of some higher-speed jetters such as adult squid (Anderson & DeMont 2000). Given that Gharib *et al.* (1998) have demonstrated the process of vortex-ring formation in starting jets to be robust up to at least a Reynolds number of 6000 (based on the circulation of the leading vortex-ring), the present results should be applicable to many of the higher-speed flows as well.

Measurement results are presented herein typically using single representative data sets for each nozzle program (figure 6 is a notable exception). Three or more iterations were conducted for each programme of nozzle exit diameter temporal variation to ensure that stated values accurately represent each test case. The maximum uncertainty in each representative data set is $\pm 5\,\%$.

2.5. *Boundary-layer dynamics*

Didden (1979) clearly demonstrated the special role of boundary-layer dynamics in the development of starting flows, especially in relation to leading vortex-ring formation. Using laser-Doppler velocimetry (LDV) measurements, he observed quantitatively how the motion of the boundary layer at flow initiation dominates the roll-up of the leading vortex-ring. In addition, boundary-layer growth within the hollow cylinder of the vortex generator was shown to lead to an increase in vorticity flux into the starting jet. These interesting aspects of starting flows cannot be captured by a simplified slug model of the flow, which neglects boundary-layer effects altogether (cf. Shariff & Leonard 1992; Krueger & Gharib 2003).

Shusser *et al.* (2002) suggested incorporating a Rayleigh–Stokes solution to account for boundary-layer growth within the hollow cylinder of a piston–cylinder vortex generator. A modified version of their solution, presented by Dabiri & Gharib (2004*b*), achieved close agreement with DPIV measurements of the generated vorticity flux.

In the present apparatus, we must address the added complexity of a spatially and temporally accelerating mean flow due to the presence of a nozzle with temporally variable contraction ratio D_p/D_e downstream of the piston–cylinder apparatus. The effect of this unsteady flow on the boundary layer that formed upstream in the piston–cylinder apparatus will largely dictate the nature of the starting flow that emerges from the nozzle exit.

A quasi-steady analysis predicts that the boundary layer entering the nozzle from the piston–cylinder apparatus will become thinner owing to the nozzle contraction, perhaps eliminating the need for the correction of Dabiri & Gharib (2004*b*) to the starting flow. However, the combination of spatial and temporal accelerations in the real starting flow adds complexity that cannot be captured easily by a quasi-steady analysis.

Our piston–cylinder flow rate data and nozzle exit velocity profile measurements obtained using DPIV are sufficient to determine the level of boundary-layer thinning achieved in each of the experiments performed here. This information will be critical for modelling these starting flows properly, especially in predicting the vorticity flux from the nozzle in each experiment.

https://doi.org/10.1017/S002211200500515X Published online by Cambridge University Press

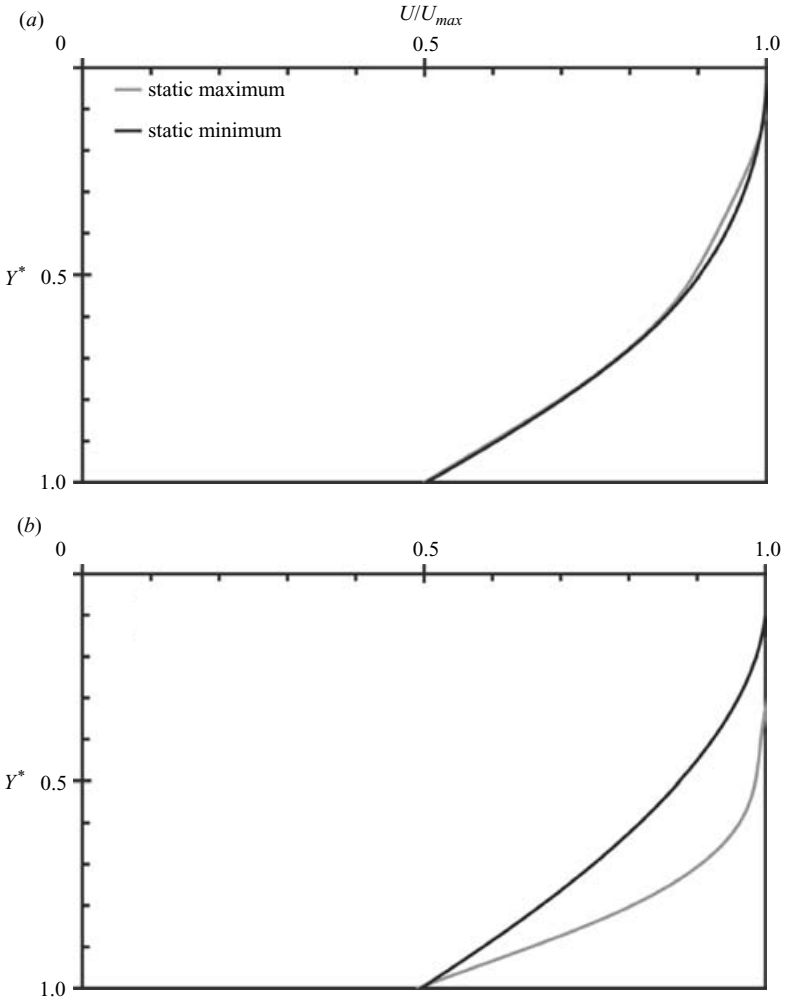


FIGURE 4. Velocity profile of fluid efflux at $X = 0.3$ D_p for static minimum and maximum diameter cases. (a) $T = 0.67$ s. (b) $T = 2.0$ s. Y^* is the radial coordinate normalized by the location at which $U/U_{max} = 0.5$.

Measurements of the exit velocity profile for each temporal pattern of nozzle diameter variation indicate that those cases with larger average nozzle contraction ratio during initiation of the starting jet (i.e. SMIN, SO and FO cases) exhibit significantly less boundary-layer thinning than those with smaller average nozzle contraction ratio over the same period of time (i.e. SMAX, SC and FC cases). Figure 4 exemplifies these trends for the SMIN and SMAX diameter cases. Initially, the boundary-layer dynamics are similar in the two cases (figure 4a). However, at later times the larger nozzle contraction ratio in the SMIN case causes boundary-layer vorticity from the upstream piston–cylinder apparatus to be convected downstream out of the nozzle faster than it is rearranged by diffusion, allowing the upstream velocity profile (i.e. at the nozzle entrance) to pass through the nozzle essentially unchanged. Thus, the velocity profile in the SMIN case does not exhibit thinning similar to that expected in a quasi-steady flow. By contrast, the SMAX case has

https://doi.org/10.1017/S002211200500515X Published online by Cambridge University Press

a smaller nozzle contraction ratio and therefore a lower spatial acceleration in the nozzle. Accordingly, upstream vorticity from the piston–cylinder apparatus persists in the nozzle for a longer duration, allowing viscous diffusion to rearrange the boundary layer. In these cases, boundary-layer thinning is more substantial (figure 4*b*).

The observed dynamics of the boundary layers in these starting flows are a consequence of the specific experimental apparatus implemented for vortex generation. We do recognize that there exist various methods to mitigate the effect of the boundary layer so that it does not play such a large role in the fluid dynamics (e.g. Joslin 1998). However, we have not aimed at implementing those strategies herein.

In the following sections we will model the starting flow for the SMAX, SC and FC nozzles as if the piston–cylinder boundary layer has completely thinned in the nozzle, while modelling the SMIN, SO and FO cases as if the piston–cylinder boundary-layer has passed through the nozzle unchanged. Although boundary-layer thinning will occur to some degree in every test case, we will show that this approximation is sufficient to generate a realistic picture of the starting flows in these experiments.

3. Results

3.1. *Vorticity flux*

The flux of vorticity from the starting flow boundary layer provides a useful measure of the dynamical contribution of the vortex generator to the ambient fluid. Measuring the flux of vorticity, in practice, typically requires a precise velocimeter, a prospect that is often inconvenient when studying biological systems or engineering technologies with auxiliary components that interfere with controlled experimental observations. It is therefore desirable to develop analytical models to predict accurately the vorticity flux from starting flows, based on known parameters of the vortex generator. Naturally, our focus is directed toward starting flows through temporally variable nozzles.

In the case of a piston–cylinder apparatus, the classical slug model result for the vorticity flux is

$$\left.\frac{\mathrm{d}\Gamma}{\mathrm{d}t}(t)\right|_{slug} \approx \tfrac{1}{2}U_p^2(t), \tag{3.1}$$

where Γ is the circulation delivered by the vortex generator and U_p is the (possibly time-dependent) piston speed.

By replacing the piston velocity with the fluid volume flux $\dot{\Omega}$ and the circular nozzle or orifice exit diameter D_e, we arrive at a generalized vorticity flux model for an arbitrary source flow with circular nozzle or orifice exit:

$$\left.\frac{\mathrm{d}\Gamma}{\mathrm{d}t}(t)\right|_{slug} \approx \frac{8\dot{\Omega}^2(t)}{\pi^2 D_e^4(t)}. \tag{3.2}$$

Boundary-layer growth inside the vortex generator results in a decreased flow velocity near the walls and concomitant increase in velocity outside the boundary layer in order to satisfy continuity. As mentioned in the previous section, only a simplified model of this process is tractable in the present context. Using the result of Dabiri & Gharib (2004*b*), the vorticity flux in this case is predicted by

$$\left.\frac{\mathrm{d}\Gamma}{\mathrm{d}t}(t)\right|_{\mathrm{BLG}} \approx \frac{8\dot{\Omega}^2(t)}{\pi^2 D_e^4(t)}\left[1+\frac{8(\nu t)^{1/2}}{\pi^{1/2}D_e(t)}\right]^2. \tag{3.3}$$

https://doi.org/10.1017/S002211200500515X Published online by Cambridge University Press

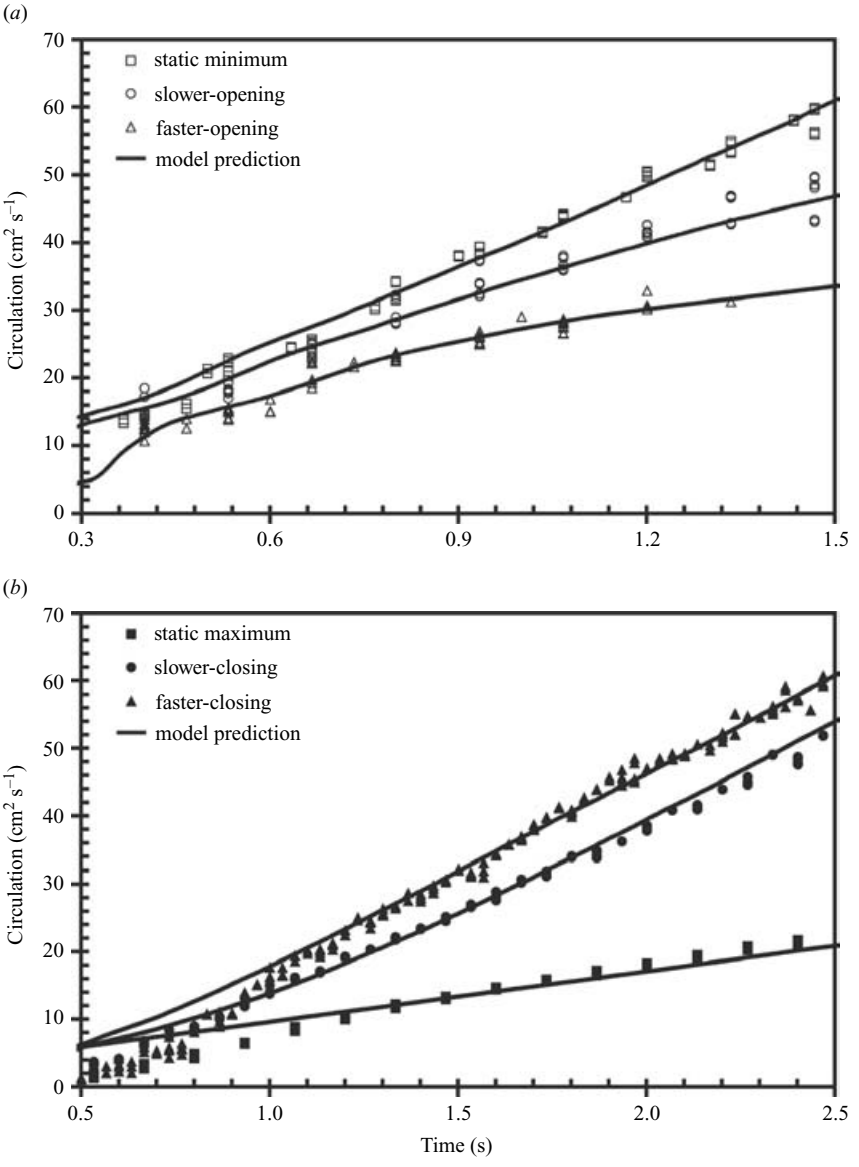


FIGURE 5. Measured and predicted circulation generated for each programme of nozzle exit diameter temporal variation. (*a*) SMIN, SO and FO cases. (*b*) SMAX, SC and FC cases.

According to the conclusions § 2, (3.2) was used to predict the vorticity flux in the SMAX, SC and FC cases, while (3.3) was applied to the SMIN, SO and FC cases. The results are plotted in figure 5. After initial vortex ring roll-up, the agreement is very good in each case, especially considering that no empirical scaling factors have been used. Discrepancies shortly after flow initiation at time $T = 0$ are due to difficulties in measuring the flow field close to the nozzle exit; and because of vortex ring roll-up and overpressure effects previously documented by Didden (1979) and Krueger (2001), which cannot be captured by these models. The former issue, which causes an uncertainty in the measured time of flow initiation, will be revisited in

https://doi.org/10.1017/S002211200500515X Published online by Cambridge University Press

the following section. Notably, the global flow – represented by the total generated circulation – is accurately predicted by the models.

3.2. *Dimensional analysis*

In preparation for the ensuing discourse on leading vortex-ring dynamics, it is useful to prepare a dimensionless framework in which to present the results. Gharib *et al.* (1998) define a vortex-ring formation time corresponding to the dimensionless length of the fluid slug ejected from a piston–cylinder apparatus:

$$T^*_{\mathrm{GRS}} \equiv \frac{\overline{U_p}t}{D_p}, \tag{3.4}$$

where the overbar denotes a running time average. Mohseni *et al.* (2001) use a modified form of this definition, in which the piston speed is replaced by the vortex-ring celerity.

The difficulty with these definitions in a general starting flow is that the former is valid strictly for a constant-diameter vortex generator, and the latter requires knowledge of the motion of the leading vortex ring, which may be inaccessible or even irrelevant to the particular flow of interest.

A generalized dynamic dimensionless time scale based on the parameters of the vortex generator can be derived by considering an infinitesimal increment in the formation time of Gharib *et al.* (1998):

$$\mathrm{d}T^* = \frac{U_e(t)}{D_e(t)}\,\mathrm{d}t. \tag{3.5}$$

In (3.5), the nozzle exit velocity U_e (i.e. the free-stream flow velocity outside the boundary layer as in Dabiri & Gharib 2004*b*) is used as the appropriate characteristic velocity instead of the piston speed. Integrating over the duration of fluid ejection, we arrive at a dimensionless time scale that properly accounts for temporal changes in the exit diameter:

$$T^* = \int_0^t \frac{U_e(\tau)}{D_e(\tau)}\,\mathrm{d}\tau = \overline{\left(\frac{U_e}{D_e}\right)}t. \tag{3.6}$$

This new dimensionless parameter is monotonically increasing for any temporal variation of the exit diameter, as it must be to accurately reflect the irreversible nature of the fluid ejection process. In contrast, definition (3.4) of Gharib *et al.* (1998) gives a spurious result of decreasing formation time when the instantaneous or time-averaged exit diameter is increasing.

Consistent with the preceding result, the circulation is properly normalized using the terms $\overline{(U_e/D_e)}$ and $\overline{U_e^2}$ as

$$\Gamma^* = \frac{\Gamma\overline{(U_e/D_e)}}{\overline{U_e^2}}. \tag{3.7}$$

Despite the inclusion of a boundary-layer correction to the exit velocity in the SMIN, SO and FO cases, a plot of normalized circulation versus formation time should still possess a slope of 1/2 in accord with the slug model equation (3.1). The slope is preserved because the boundary-layer correction appears in both the circulation and time normalizations, leaving their ratio unaffected. Figure 6 shows the circulation trends from several iterations of each nozzle case. The data are shifted along the abscissa so that the linear portion of each trend has its intercept at the origin. After initial scatter, all of the data collapse to the reference line with slope equal to 1/2.

https://doi.org/10.1017/S002211200500515X Published online by Cambridge University Press

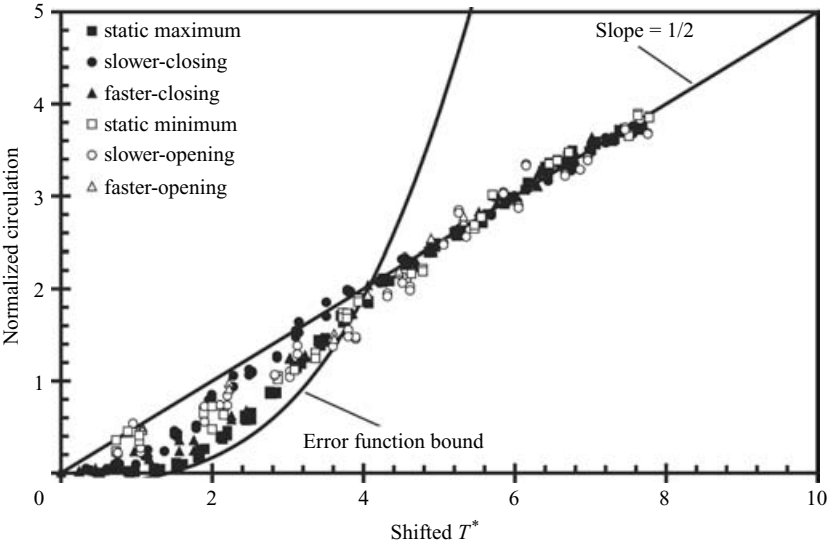


FIGURE 6. Normalized circulation versus formation time for each programme of nozzle exit diameter temporal variation. Solid lines indicate slope = 1/2 and error function bound.

Data scatter at early formation time is largely due to differences in the manner in which the leading vortex ring enters the DPIV measurement window from the upstream boundary at $X = 0.3D_p$. The trend of increasing measured circulation during this time is dominated by propagation of the vortex-ring core vorticity into the measurement window at the upstream boundary. Hence, the measured data trends at early formation time are not necessarily indicative of the actual rate of vorticity generation by the starting flow. This effect has been previously observed by Didden (1979) using LDV measurements and Dabiri & Gharib (2004*b*) using DPIV. Since this effect occurs well before vortex ring pinch-off, it is an artefact with little influence on the measurements of importance to these experiments. Nonetheless, we can quantitatively bound this effect by assuming that the vortex cores possess a Gaussian vorticity distribution and enter the measurement window in a quasi-steady fashion. The fluid circulation entering the measurement window owing to this motion will then be an error function of time by definition, since the circulation measurement is the definite integral of an assumed normal distribution of vorticity (centred at the vortex core) over the finite spatial region $0.3D_p \leqslant X \leqslant 6.2D_p$. Figure 6 indicates one such curve that effectively bounds the scatter in these experiments.

As an aside, the reader may be tempted to correlate the observed intersection of the linear and error function curves in figure 6 to the fact that pinch-off typically occurs at this same location in the space of normalized circulation versus formation time (i.e. $[T^*, \Gamma^*] = [4, 2]$). We strongly suggest that this is merely a coincidence in the present case. This conclusion is supported by the fact that, as previously mentioned, the data has been artificially shifted in formation time to force the linear trends to intersect the origin. In addition, the error function curve chosen to represent the lower bound of data scatter will change depending on the location of the upstream boundary of the measurement window. These choices are completely independent of the dynamics of leading vortex-ring pinch-off.

https://doi.org/10.1017/S002211200500515X Published online by Cambridge University Press

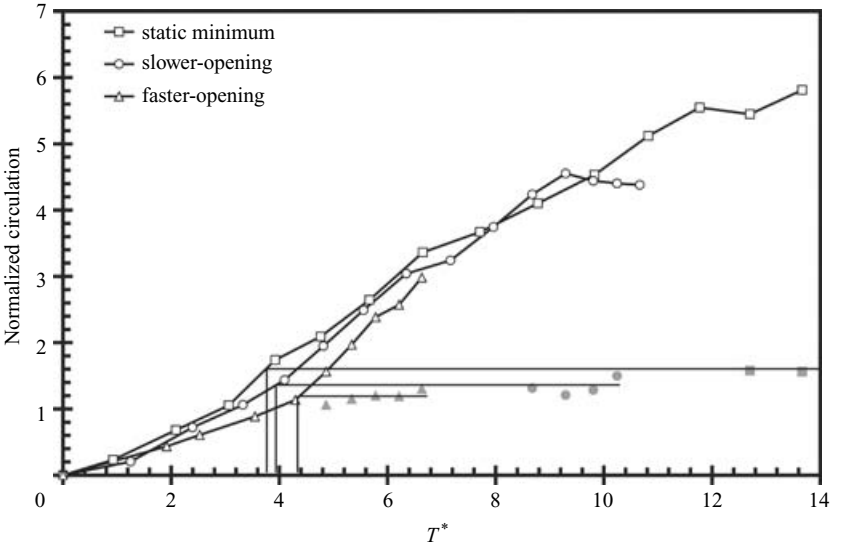


FIGURE 7. Normalized circulation versus formation time for SMIN, SO and FO cases. Grey symbols indicate circulation of leading vortex ring after pinch-off.

3.3. *Leading vortex-ring pinch-off and vorticity distribution*

With a dimensionless perspective on the fluid dynamics in place, we are prepared to examine the physics of leading vortex-ring pinch-off. To reiterate, our focus on the pinch-off process is motivated by its dynamical significance as discovered by Krueger (2001), and the possibility of generating vortex rings of low dimensionless energy as implied by the results of Mohseni *et al.* (2001).

The method of Gharib *et al.* (1998) is used to determine the dimensionless vortex formation time corresponding to the onset of pinch-off, i.e. the formation number F. By measuring the circulation of the leading vortex ring after pinch-off, the formation time at which this circulation was generated by the starting flow is found. Figure 7 plots the dimensionless circulation versus formation time for the SMIN, SO and FO nozzle cases. The formation time at the onset of pinch-off consistently falls between 3.7 and 4.4 for each group. These data are in agreement with the range observed by Gharib *et al.* (1998). Contrary to the prediction of Mohseni *et al.* (2001), we do not observe a significant delay in vortex-ring pinch-off for the cases with temporally increasing nozzle exit diameter. Our finding is consistent with the results of Allen, who also did not observe a beneficial effect of a temporally increasing exit diameter on vortex-ring formation. Further examination of the leading vortex-ring vorticity profile for each case provides the insight necessary to understand why the method has been ineffective. Figure 8 plots the vorticity profile along a radial section of the leading vortex-ring at the formation number. For the SMIN case, the core vorticity distribution is qualitatively similar to a Gaussian-type profile. When the nozzle exit diameter is increased temporally as the starting flow emerges, the locations of peak core vorticity and the core vorticity centroid are both moved radially away from the axis of symmetry, as Mohseni *et al.* (2001) predicted. Furthermore, the radial motions of the vorticity peak and centroid occur nearly in direct proportion to the radial motion of the nozzle exit diameter.

However, in each case the portions of the shear layer closer to the axis of symmetry are unaffected by the nozzle motion; the near-axis vorticity consistently extends to

https://doi.org/10.1017/S002211200500515X Published online by Cambridge University Press

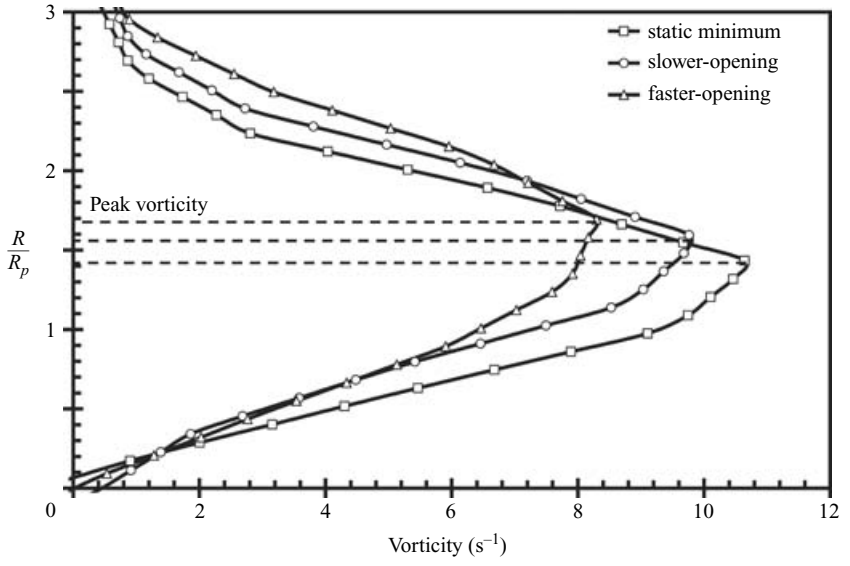


FIGURE 8. Vorticity profile along the radial section of the vortex ring core for SMIN, SO and FO cases. Dashed lines indicate the location of peak vorticity in each profile.

the symmetry axis at the same formation time as the static nozzle case. We can conclude that although the temporal increase in nozzle exit diameter was effective in manipulating the radial location of peak vorticity in the core, the nozzle motion was insufficient to prevent the entire shear layer from encroaching on the axis of symmetry. Movement of the entire shear layer away from the centreline is necessary to delay vortex-ring pinch-off.

The present results may be attributed in part to the thickness of the shear layer at the relatively low Reynolds numbers of these experiments. We remain open to the possibility that at much higher Reynolds numbers, the shear layer might be sufficiently thin that it uniformly follows the motion of the vorticity peak. A more general discussion of dynamical benefits of the temporally increasing nozzle exit diameter is reserved for the concluding section of this paper.

Circulation data for the SMAX, SC and FC nozzle cases is shown in figure 9. In the absence of nozzle motion (i.e. SMAX case), leading vortex-ring pinch-off occurs at a maximum formation number of 4.6. This is reasonably consistent with the range reported by Gharib *et al.* (1998). When a temporally decreasing nozzle exit diameter is introduced, the formation number increases substantially, to 6.9 for the SC case and to 8.0 for the FC case. This delay in vortex-ring pinch-off is dramatically greater than that achieved by Dabiri & Gharib (2004*a*) using an external bulk counterflow. Normalized circulation of the leading vortex ring is also increased by up to 35 % over the static nozzle case.

For consistency with the preceding analysis, we plot the vorticity distribution along a radial section of the vortex ring core for the SMAX, SC and FC cases at the formation number (figure 10). Unlike the trend observed for the radially increasing exit diameter, the radially decreasing exit diameter has little effect on the location of peak vorticity or the core vorticity centroid. There is, however, a large change in the magnitude of peak vorticity. The FC nozzle case exhibits peak vorticity at nearly double the peak level of the static nozzle. In addition, the temporally decreasing exit

https://doi.org/10.1017/S002211200500515X Published online by Cambridge University Press

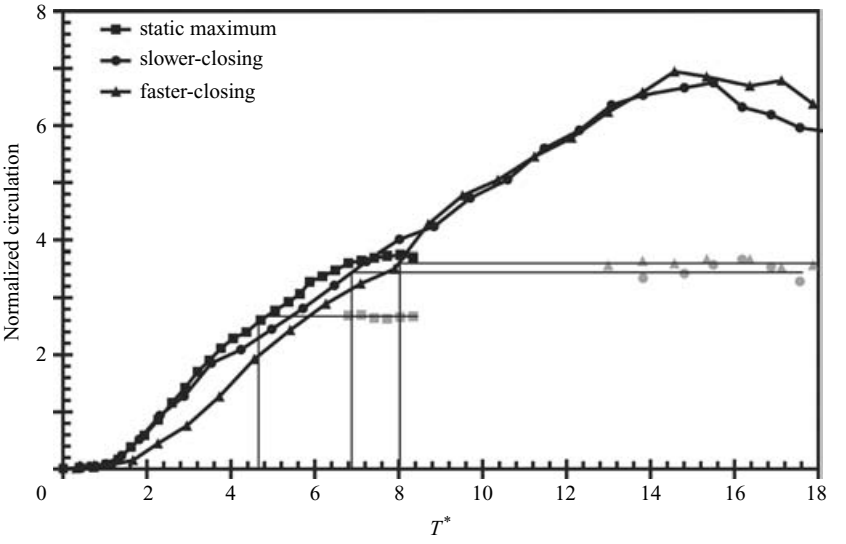


FIGURE 9. Normalized circulation versus formation time for SMAX, SC and FC cases. Grey symbols indicate circulation of the leading vortex ring after pinch-off.

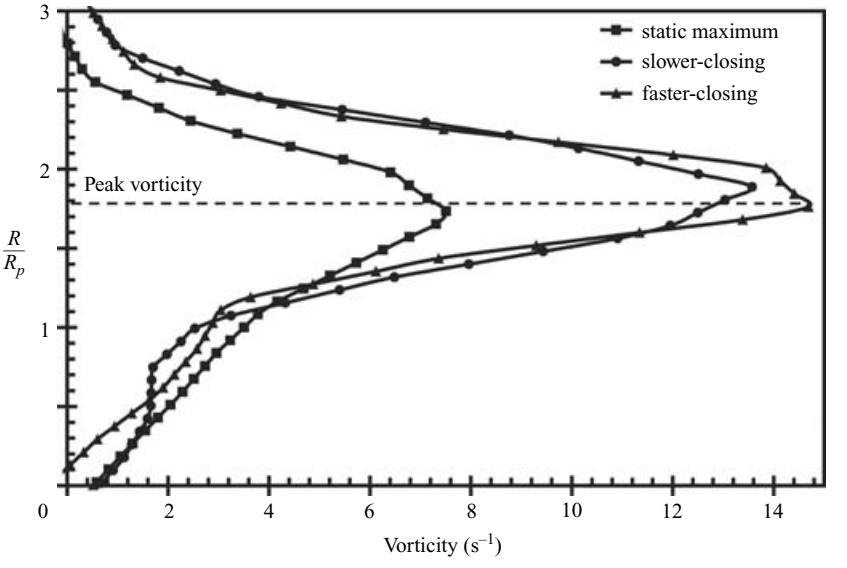


FIGURE 10. Vorticity profile along the radial section of the vortex ring core for SMAX, SC and FC cases. Dashed line indicates approximate location of peak vorticity in each profile.

diameter nozzle cases possess a distinct discontinuity in the slope of the vorticity distribution approximately $1R/R_p$ from the axis of symmetry.

The vortex dynamics leading to these observed pinch-off and vorticity distribution trends are best explained in the context of a discourse on the leading vortex-ring energy, as follows.

https://doi.org/10.1017/S002211200500515X Published online by Cambridge University Press

3.4. *Leading vortex-ring energy*

The dimensionless vortex-ring energy E^* is an especially useful parameter for investigating the dynamics of these starting flows, as it invokes the dynamical invariants being delivered from the vortex-generator. Measuring the vortex-ring energy is difficult, in practice, because it requires powers, quotients and integrals of the velocity and vorticity fields:

$$E^* = \frac{E}{I^{1/2}\Gamma^{3/2}} = \frac{\pi \int \omega\psi \, \mathrm{d}x \, \mathrm{d}r}{\left[\pi \int \omega r^2 \, \mathrm{d}x \, \mathrm{d}r\right]^{1/2} \left[\int \omega \, \mathrm{d}x \, \mathrm{d}r\right]^{3/2}}, \tag{3.8}$$

where E, I and Γ are the dimensional energy, impulse and circulation, respectively and ψ is the streamfunction. The velocity and vorticity fields have been measured with non-zero error, which will subsequently compound when computing the dimensionless energy. An additional source of uncertainty arises in selection of the vorticity contour that will be used to define the vortex core. Definitions of the vortex core based on a given vorticity contour level are *ad hoc*, and make comparison between different cases somewhat tenuous.

A reliable method of obtaining the leading vortex-ring energy is indicated in Gharib *et al.* (1998). As dictated by the Kelvin–Benjamin variational principle, we can exploit the fact that the leading vortex-ring energy is equal to the instantaneous energy of source flow delivered by the vortex generator at the formation number.

Using this strategy, we first revisit the pinch-off results for nozzle cases with temporally increasing exit diameter. Figure 11(*a*) plots the dimensionless energy supplied by the vortex generator in the SMIN, SO and FO cases (using the exit velocity $U_e(t)$ to compute source flow impulse and energy), along with the leading vortex-ring energy. For the SMIN case, the dimensionless energy of the leading vortex-ring is 0.40. This value is higher than that found by Gharib *et al.* (1998) but in the range of Mohseni *et al.* (2001) for vortex rings with similar normalized circulation. Movement of the peak vorticity away from the axis of symmetry by the nozzle motion results in vortex-ring vorticity distributions with larger normalized energy, over 0.5 for the FO nozzle.

Nozzles with temporally increasing exit diameter successfully deliver source flow at higher dimensionless energy than the static nozzle case. Gharib *et al.* (1998) predict that this condition of increased dimensionless energy from the vortex generator is necessary in order to achieve a delay in pinch-off of the leading vortex-ring. However, in the present experiments the concomitant increase in leading vortex-ring energy due to vorticity redistribution (namely, radial movement of the core vorticity peak and centroid) negates any potential benefit from the increased energy source. If the source flow could be delivered at the same elevated energy level without affecting the leading vortex-ring vorticity distribution, a substantial delay in vortex-ring pinch-off might be achieved.

The dynamics of the SC and FC cases are more complex. In these nozzle cases, we observed substantial increases in the formation number and the normalized circulation of the leading vortex ring. One of two effects (or perhaps a combination thereof) can be expected to play a role in the augmented starting-flow dynamics. In the first case, we might suspect that the increasing source flow velocity enables delay of leading vortex-ring pinch-off, as predicted by Shusser & Gharib (2000) and Mohseni *et al.* (2001). Alternatively, the nozzle motion may have induced a change in the distribution of vortex-ring vorticity, resulting in a lower dimensionless energy of the leading vortex

https://doi.org/10.1017/S002211200500515X Published online by Cambridge University Press

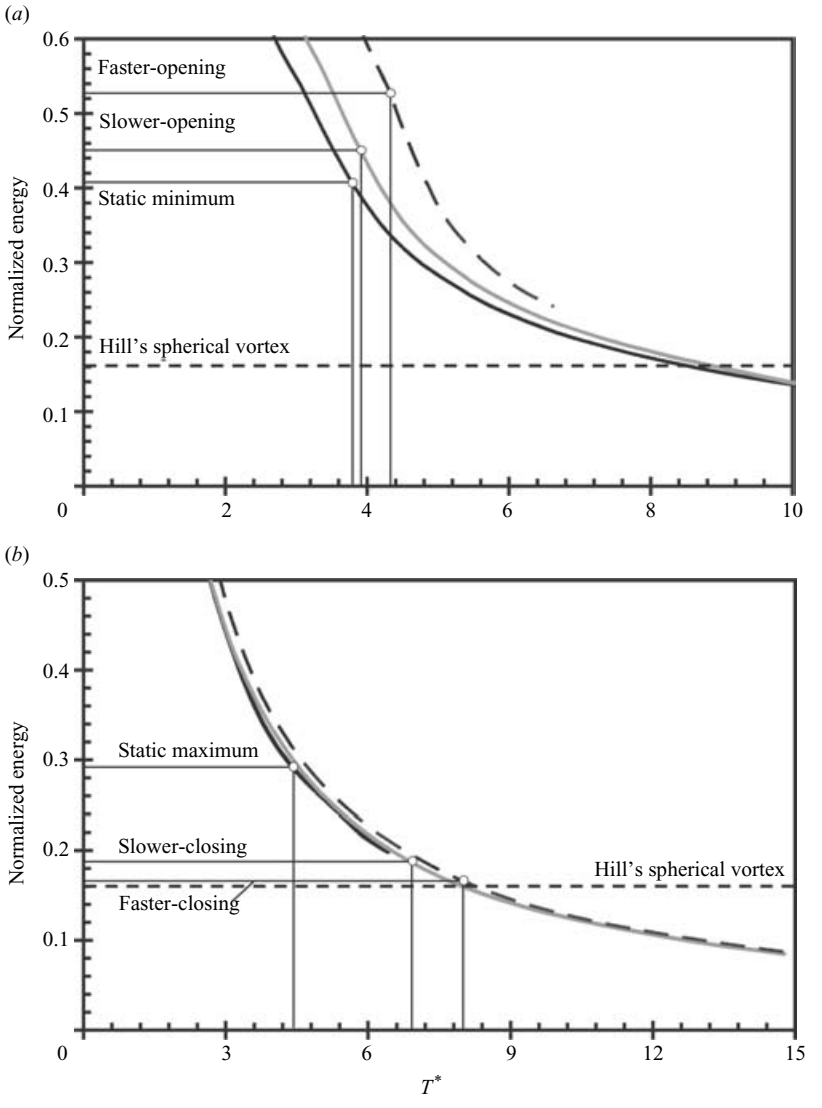


FIGURE 11. Normalized vortex generator energy versus formation time. Encircled points in each plot indicate leading vortex-ring energy. (*a*) SMIN, SO and FO cases. (*b*) SMAX, SC and FC cases.

ring and an associated decrease in the required source flow energy to sustain ring growth.

Figure 11(*b*) indicates that the latter of these two effects is present. Unlike the temporally increasing nozzle exit diameter, the temporally decreasing cases have little effect on the dimensionless energy carried by source flow from the vortex generator. Hence, we can conclude that it is changes in the vortex ring vorticity distribution that have led to the observed delay in vortex-ring pinch-off, and not some characteristic of the source flow such as its velocity.

The development of the leading vortex-ring vorticity distribution in temporally decreasing nozzle exit diameter cases is distinct from both the static nozzle and the temporally increasing nozzle exit diameter cases. Vorticity contours of the normal

https://doi.org/10.1017/S002211200500515X Published online by Cambridge University Press

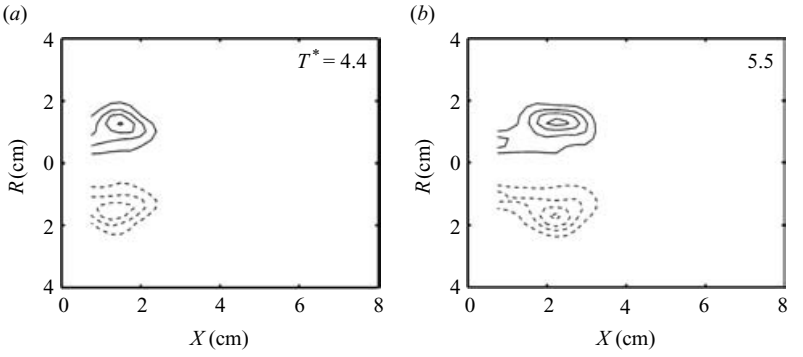


FIGURE 12. Vorticity contours of the flow downstream of the static maximum diameter nozzle. Flow is from left to right. Solid and dashed lines indicate positive and negative vorticity, respectively. Contour spacing is $2\,s^{-1}$.

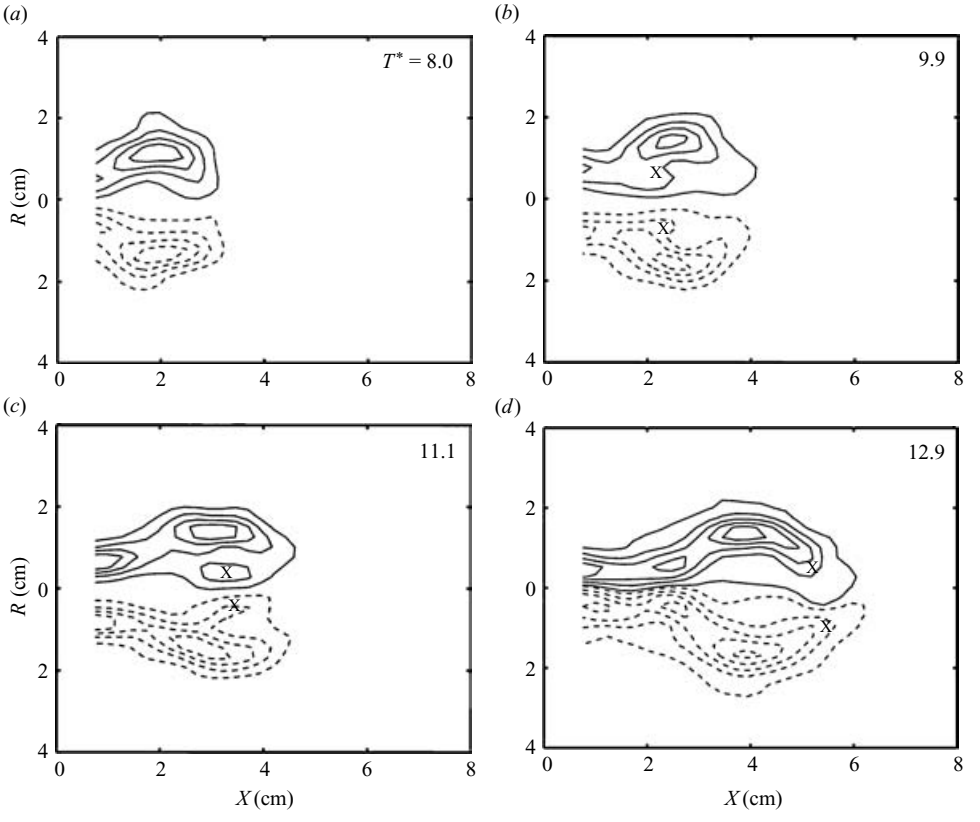


FIGURE 13. Vorticity contours of the flow downstream of the FC diameter nozzle. Flow is from left to right. Solid and dashed lines indicate positive and negative vorticity, respectively. Contour spacing is $3\,s^{-1}$. Downstream convection of vorticity along the axis of symmetry is tracked by a cross symbol placed at the local vorticity peak.

process are shown in figure 12, just before and after pinch-off from the SMAX nozzle. The shear-layer efflux behaves in the expected fashion, emerging parallel to the axis of symmetry and possessing a larger region of concentrated vorticity in the leading vortex-ring core. In the case of nozzle exit diameter contraction (figure 13), the

https://doi.org/10.1017/S002211200500515X Published online by Cambridge University Press

vorticity flux is ejected closer to the axis of symmetry as time progresses. A portion of this vorticity is convected axially toward the front stagnation point of the starting flow by the circulatory motion of the leading vortex ring. Figures 13(*b*)–13(*d*) track the vorticity travelling from the rear of the ring to the front stagnation point. The remainder of the shear-layer efflux left behind the leading vortex ring interacts with its mirror image across the axis of symmetry, contributing to the disconnection of the leading vortex ring.

Crescent-shaped vorticity patches arise in the leading vortex ring after this process (e.g. figure 13*d*), in contrast with the typical elliptic patches. In the preceding section, the vorticity distribution near the axis of symmetry was noted to display a trend different from the typical Gaussian profile. From figure 13, we can now see that this effect is due to the shear-layer vorticity that was fed close to the axis of symmetry and subsequently passed from the rear of the ring to the front stagnation point. The motion of this vorticity also appears to have prevented the leading vortex-ring cores from following the nozzle wall motion toward the axis of symmetry, as was observed (in the opposite sense) in the temporally increasing nozzles. This explains the difference in the dynamics of the vorticity peaks plotted in figures 8 and 10.

Vortex rings with very low dimensionless energy are generated by the process described above. Starting flow through the FC nozzle formed leading vortex rings with dimensionless energy equal to 0.165 ± 0.009. This value agrees with direct measurements using (3.8), which gave values in the range of 0.16 ± 0.02. For comparison, Hill's spherical vortex has a dimensionless energy of 0.160. The vortex rings generated in the present experiments are not Hill's vortices, however, because the vorticity distribution is not uniformly linear in the radial direction. Furthermore, the rings could potentially have dimensionless energy lower than that of Hill's vortex, as demonstrated by Mohseni *et al.* (2001) for vortex rings formed at low Reynolds numbers (i.e. less than 1000 based on the leading vortex-ring circulation). Nonetheless, the comparison with Hill's vortex is noteworthy because previous analytical studies of the pinch-off process have invoked the Norbury family of vortices, which includes Hill's vortex as its limiting member (e.g. Gharib *et al.* 1998; Linden & Turner 2001; Mohseni *et al.* 2001). In particular Linden & Turner (2001) predict that vortex rings with dimensionless energy equal to Hill's vortex can be achieved by a constant-diameter piston–cylinder apparatus if pinch-off is delayed until a dimensionless vortex formation time of 7.83. That predicted pinch-off time is very close to the values observed here for vortex rings with Hill-type dimensionless energy formed by the FC nozzle.

3.5. *Leading vortex-ring fluid transport*

Finally, we present an aspect of starting-flow dynamics that is largely absent from the literature; namely, the issue of how much fluid is transported by the leading vortex ring of the starting flow. Although the preceding sections have identified effective means of delaying pinch-off and producing vortex rings with low dimensionless energy and high normalized circulation, we must ask if there is any penalty being paid in the process of mass transfer relative to the static nozzle cases. Since the volume flux through each nozzle is identical, such a comparison can be made given the available data.

Figure 14 plots the volume of source flow carried in the leading vortex ring of each starting flow through a temporally variable nozzle exit diameter, $\Omega(t)$, relative to its static nozzle counterpart at pinch-off Ω_0. Temporal increases in the nozzle exit diameter have a minor effect on the volume of fluid transported by the leading vortex

https://doi.org/10.1017/S002211200500515X Published online by Cambridge University Press

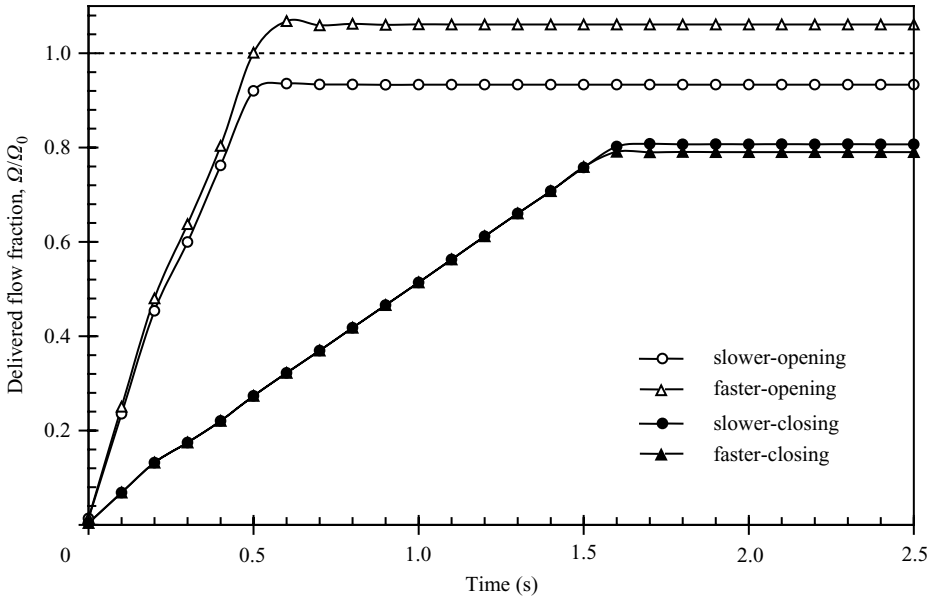


FIGURE 14. Delivered fluid fraction for leading vortex rings in nozzle cases with temporally variable exit diameter.

Nozzle program	Formation number	Pinch-off time (s)	Vortex circulation ($cm^2\ s^{-1}$)	Vortex diameter (cm)
SMIN	3.7	0.57	17.5	3.6
SO	3.9	0.53	14.5	4.1
FO	4.3	0.60	13.4	4.3
SMAX	4.6	1.95	17.9	4.4
SC	6.9	1.56	30.2	4.8
FC	8.0	1.54	32.8	4.5

TABLE 1. Dimensional parameters of the leading vortex ring for each nozzle program. Values are representative and possess a maximum uncertainty of $\pm 5\,\%$.

ring. In contrast, the temporally decreasing nozzle exit cases deliver only 80 % of the fluid that the static nozzle is capable of transporting via the leading vortex ring. The practical significance of this performance limit will depend on the details of a particular application, especially the expense of reciprocating the motion to generate additional vortex rings. Nonetheless, this result clearly demonstrates the need to examine starting-flow performance from several perspectives, both dimensional and independent of physical units.

Table 1 summarizes relevant dimensional parameters of the leading vortex rings measured in each test case. These data complement the dimensionless perspective commonly taken to study the dynamics of vortex-ring pinch-off.

4. Summary and conclusions

This paper has described a detailed experimental study of starting flow through nozzles with temporally variable exit diameter. Our strategy has been to decouple the

https://doi.org/10.1017/S002211200500515X Published online by Cambridge University Press

source flow from the nozzle dynamics in order to successfully facilitate comparison among various classes of nozzle motion.

An important tool in these analyses has been the use of a dimensionless perspective on the evolution of the starting flows. We have defined a new parameter to track the temporal development of the dynamics, which properly accounts for the effect of a temporally variable exit diameter. Improved kinematic models based on a generalized description of the source flow are demonstrably successful in predicting the circulation delivered by the vortex generator after initial vortex-ring roll-up. These models have also helped to emphasize the important contribution of the boundary layer to starting-flow dynamics.

Several previously unresolved questions regarding the nature of the leading vortex ring in starting flows have been answered or at least refined, through a study of the pinch-off process and vortex ring vorticity distribution and energy. We have shown that temporally increasing the nozzle exit diameter as the starting flow emerges leads to a measurable increase in the radial location of peak vorticity in the leading vortex ring. Consequently, the energy of the leading vortex ring is increased. Since the energy delivered by the vortex generator is also increased in the process, the two effects counteract one another, preventing a change in the normalized circulation of the leading vortex ring or the dimensionless time at which pinch-off occurs.

These experiments have demonstrated the ability of a temporally decreasing nozzle exit to facilitate substantial increases in the formation number and normalized circulation of the leading vortex ring. In the process, vortex rings with very low normalized energy were produced. Examination of the vorticity contours revealed a unique transient effect during development of these starting flows, in which vorticity from the trailing shear layer was forced through the centre of a forming vortex ring by the nozzle motion and induced velocity of the ring.

Finally, we have briefly discussed the concept of dimensional fluid transport by the leading vortex ring, to demonstrate a trade-off that may possibly exist between energetic improvements to the starting-flow process and the ability of the flow to facilitate mass transfer.

The existing work related to this specific problem is limited; however, the present results are consistent in principle with those previous findings. It has been observed here that the prediction of Mohseni *et al.* (2001) of thick vortex-ring generation by increasing the spatial extent of flow forcing may possibly be achieved, if the shear-layer efflux is sufficiently thin that it behaves uniformly with the vorticity peak. In the present experiments, the spatially increasing nozzle motions effectively actuated the location of peak vorticity, however, the shear layer was too thick to prevent encroachment of the near-axis vorticity on the centreline. Allen appears to have also been unable to prevent this from occurring with his apparatus.

These experiments indicate that the benefit of a temporally decreasing nozzle diameter for generation of thick low-energy vortex rings is related to changes in the vorticity distribution of the forming leading vortex ring that are induced by the nozzle motion. Although we suggest that this mechanism is dynamically distinct from the alternative explanation based on the velocity of the trailing source flow (e.g. Shusser & Gharib 2000; Mohseni *et al.* 2001), it could be reasonably argued that the two effects are similar from a kinematic perspective. Again, these results are at least qualitatively in agreement with the observations of Allen.

It is prudent to discuss the limitations of the experimental techniques and strategy employed herein. Perhaps the most immediate observation is that these experiments have all been conducted with a single nozzle-type exit geometry. Given that the

https://doi.org/10.1017/S002211200500515X Published online by Cambridge University Press

vortex-ring trajectory can be influenced by the nature of the vortex-generator exit boundary conditions (e.g. nozzle or orifice; Auerbach 1987), the quantitative trends measured in the present work may be adjusted for other exit geometries. This is especially true in the application of these results to biological systems, many of which also deviate from axisymmetry in the exit shape. Two common examples are the lappets at the bell margin of many schyphozoan jellyfish (e.g. Dabiri & Gharib 2003) and the funnels of some squids (e.g. Anderson & DeMont 2000).

Fluid continuity demands that our decision to decouple the source flow volume flux from the nozzle motion must be paid for in a new coupling between the diameter and flow velocity at the nozzle exit plane. This could potentially complicate interpretation of the results, since the exit plane velocity will be decreasing as the exit diameter increases and *vice versa*.

The plots of dimensionless energy in figure 11 confirm that this was not an important factor in the present experiments. Despite the decrease in nozzle exit plane velocity while the exit diameter was increasing, we see that the delivered energy still increased, following the trend commanded by the nozzle exit diameter (figure 11*a*). Similarly, despite the relatively large increase in nozzle exit velocity while the exit diameter was decreasing, the delivered energy remained unaffected (figure 11*b*).

We conclude with a brief summary of some anticipated benefits of temporal variation of the exit diameter during pulsatile flow generation, based on the results of this study. Temporal increases in the exit diameter will be primarily useful for enhancing the impulse delivered by the vortex-generator source flow, at the expense of ejection efficiency. In addition, the corresponding increase in the radial extent of the leading vortex-ring cores can provide substantial augmentation of ambient fluid entrainment by the starting flow, facilitating transfer of the impulse to a greater volume of fluid (Dabiri & Gharib 2004*c*). This strategy will be useful in systems that occasionally require rapid momentum or mass transport at high cost (i.e. energy input), such as the escape mechanism of squid and cardiac pumping at elevated heart rates associated with systemic stress.

Temporal decreases in the nozzle exit diameter during flow initiation will increase efficiency of the flow ejection process, as measured by the impulse carried in each vortex ring per unit of energy expended. Systems requiring robust high-efficiency performance will benefit from this strategy. These experiments have demonstrated that the volume of fluid delivered in each vortex ring is reduced for this class of nozzle motion. However, the enhanced efficiency will facilitate additional iterations of the ejection mechanism in order to compensate without severe penalty. The measured kinematics of jellyfish swimming are consistent with this strategy, although empirical measurements of locomotive efficiency have not yet been achieved for these animals.

In the final analysis, these experiments have conclusively demonstrated potential dynamical benefits from both spatially increasing and decreasing classes of temporal nozzle exit diameter variation. Many of the trends observed here cannot be predicted by quasi-steady analysis – unsteady mechanisms must be considered. Optimal nozzle actuation will be dictated by the particular application of interest and external constraints imposed on the design of the vortex generator. We have shown here that the search for these optimal points can lead to substantial improvements in system performance.

The authors acknowledge enlightening and informative discussions with M. H. Dickinson, M. Milano, T. S. Pottebaum, A. E. Staples and J. J. Allen. We also thank

https://doi.org/10.1017/S002211200500515X Published online by Cambridge University Press

the three referees of this manuscript for their helpful suggestions. This research was conducted with the support of National Science Foundation Grant 0309671.

REFERENCES

Adrian, R. J. 1991 Paricle-imaging techniques for experimental fluid-mechanics. *Annu. Rev. Fluid Mech.* **23**, 261–304.

Anderson, E. J. & DeMont, M. E. 2000 The mechanics of locomotion in the squid Loligo pealei: locomotory function and unsteady hydrodynamics of the jet and intramantle pressure. *J. Exp. Biol.* **203**, 2851–2863.

Auerbach, D. 1987 Experiments on the trajectory and circulation of the starting vortex. *J. Fluid Mech.* **183**, 185–198.

Bartol, I. K., Patterson, M. R. & Mann, R. 2001 Swimming mechanics and behavior of the shallow-water brief squid Lolliguncula brevis. *J. Exp. Biol.* **204**, 3655–3682.

Benjamin, T. B. 1976 The alliance of practical and analytical insights into the non-linear problems of fluid mechanics. In *Applications of Methods of Functional Analysis to Problems in Mechanics* (ed. P. Germain & B. Nayroles). Lecture Notes Mathematics **503**, 8–28.

Dabiri, J. O. & Gharib, M. 2003 Sensitivity analysis of kinematic approximations in dynamic medusan swimming models. *J. Exp. Biol.* **206**, 3675–3680.

Dabiri, J. O. & Gharib, M. 2004*a* Delay of vortex ring pinch-off by an imposed bulk counter-flow. *Phys. Fluids* **16**, L28–L30.

Dabiri, J. O. & Gharib, M. 2004*b* A revised slug model boundary layer correction for starting jet vorticity flux. *Theor. Comput. Fluid Dyn.* **17**, 293–295.

Dabiri, J. O. & Gharib, M. 2004*c* Fluid entrainment by isolated vortex rings. *J. Fluid Mech.* **511**, 311–331.

Daniel, T. L. 1983 Mechanics and energetics of medusan jet propulsion. *Can. J. Zool.* **61**, 1406–1420.

Didden, N. 1979 Formation of vortex rings – rolling-up and production of circulation. *Z. Angew. Math. Phys.* **30**, 101–116.

Gharib, M., Rambod, E. & Shariff, K. 1998 A universal time scale for vortex ring formation. *J. Fluid Mech.* **360**, 121–140.

Glezer, A. & Amitay, M. 2002 Synthetic jets. *Annu. Rev. Fluid Mech.* **34**, 503–529.

Gorman, J. H. III, Gupta, K. B., Streicher, J. T., Gorman, R. C., Jackson, B. M., Ratcliffe, M. B., Bogen, D. K. & Edmunds, L. H. Jr. 1996 Dynamic three-dimensional imaging of the mitral valve and left ventricle by rapid sonomicrometry array localization. *J. Thorac. Cardiovasc. Surg.* **112**, 712–726.

Handke, M., Heinrichs, G., Beyersdorf, F., Olschewski, M., Bode, C. & Geibel, A. 2003 *In vivo* analysis of aortic valve dynamics by transesophageal 3-dimensional echocardiography with high temporal resolution. *J. Thorac. Cardiovasc. Surg.* **125**, 1412–1419.

Joslin, R. D. 1998 Aircraft laminar flow control. *Annu. Rev. Fluid Mech.* **30**, 1–29.

Kelvin, W. T. 1875 Vortex statics. *Collected works*, vol. 4, pp. 115–128. Cambridge University Press.

Krueger, P. S. 2001 The significance of vortex ring formation and nozzle exit over-pressure to pulsatile jet propulsion. PhD thesis, California Institute of Technology, Pasadena, CA.

Krueger, P. S. & Gharib, M. 2003 The significance of vortex ring formation to the impulse and thrust of a starting jet. *Phys. Fluids* **15**, 1271–1281.

Krutzsch, C.-H. 1939 Über eine experimentell beobachtete Erscheinung an Wirbelringen bei ihrer translatorischen Bewegung in wirklichen Flüssigkeiten. *Annln. Phys.* **35**, 497–523.

Linden, P. F. & Turner, J. S. 2001 The formation of 'optimal' vortex rings, and the efficiency of propulsion devices. *J. Fluid Mech.* **427**, 61–72.

Mohseni, K. 2001 Statistical equilibrium theory for axisymmetric flows: Kelvin's variational principle and an explanation for the vortex ring pinch-off process. *Phys. Fluids* **13**, 1924–1931.

Mohseni, K. & Gharib, M. 1998 A model for universal time scale of vortex ring formation. *Phys. Fluids* **10**, 2436–2438.

Mohseni, K., Ran, H. Y. & Colonius, T. 2001 Numerical experiments on vortex ring formation. *J. Fluid Mech.* **430**, 267–282.

Rosenfeld, M., Rambod, E. & Gharib, M. 1998 Circulation and formation number of laminar vortex rings. *J. Fluid Mech.* **376**, 297–318.

https://doi.org/10.1017/S002211200500515X Published online by Cambridge University Press

Rosenhead, L. 1963 *Laminar Boundary Layers*. Clarendon.

Saffman, P. G. 1978 The number of waves on unstable vortex rings. *J. Fluid Mech.* **84**, 625–639.

Shariff, K. & Leonard, A. 1992 Vortex rings. *Annu. Rev. Fluid Mech.* **24**, 235–279.

Shariff, K., Verzicco, R. & Orlandi, P. 1994 A numerical study of 3-dimensional vortex ring instabilities – viscous corrections and early nonlinear stage. *J. Fluid Mech* **279**, 351–375.

Shusser, M. & Gharib, M. 2000 Energy and velocity of a forming vortex ring. *Phys. Fluids* **12**, 618–621.

Shusser, M., Gharib, M., Rosenfeld, M. & Mohseni, K. 2002 On the effect of pipe boundary layer growth on the formation of a laminar vortex ring generated by a piston/cylinder arrangement. *Theor. Comput. Fluid Dyn.* **15**, 303–316.

Vogel, S. 1988 *Life's Devices*. Princeton University Press.

Vogel, S. 1994 Nature's pumps. *Am. Sci.* **82**, 464–471.

Widnall, S. E., Bliss, D. B. & Tsai, C.-Y. 1974 The instability of short waves on a vortex ring. *J. Fluid Mech.* **66**, 35–47.

Widnall, S. E. & Tsai, C.-Y. 1977 The instability of the thin vortex ring of constant vorticity. *Phil. Trans. R. Soc.* A **287**, 273–305.

Willert, C. E. & Gharib, M. 1991 Digital particle image velocimetry. *Exps. Fluids* **10**, 181–193.

Yogonathan, A. P., Lemmon, J. D. & Ellis, J. T. 2002 Heart valve dynamics. In *The Biomedical Engineering Handbook*. CRC Press LLC.

Zhao, W., Frankel, S. H. & Mongeau, L. G. 2000 Effects of trailing jet instability on vortex ring formation. *Phys. Fluids* **12**, 589–596.

https://doi.org/10.1017/S002211200500515X Published online by Cambridge University Press